Stretching of DNA confined in nanochannels with charged walls

Chiara Manneschi,[1,2,a)] Paola Fanzio,[3] Tapio Ala-Nissila,[4] Elena Angeli,[3] Luca Repetto,[3] Giuseppe Firpo,[3] and Ugo Valbusa[3]
[1]*Institute of Electronics, Computer and Telecommunication Engineering, National Research Council, IEIIT-CNR, Via De Marini 6, 16149 Genova, Italy*
[2]*Italian Institute of Technology, Via Morego 30, 16163 Genova, Italy*
[3]*Nanomed Labs, Department of Physics, University of Genova, via Dodecaneso 33, 16146 Genova, Italy*
[4]*Department of Applied Physics and COMP Center of Excellence, Aalto University School of Science, P.O. Box 11100, FIN-00076 Aalto, Espoo, Finland and Department of Physics, Brown University, Providence, Rhode Island 02912-1843, USA*

(Received 4 September 2014; accepted 1 December 2014; published online 10 December 2014)

There is currently a growing interest in control of stretching of DNA inside nanoconfined regions due to the possibility to analyze and manipulate single biomolecules for applications such as DNA mapping and barcoding, which are based on stretching the DNA in a linear fashion. In the present work, we couple Finite Element Methods and Monte Carlo simulations in order to study the conformation of DNA molecules confined in nanofluidic channels with neutral and charged walls. We find that the electrostatic forces become more and more important when lowering the ionic strength of the solution. The influence of the nanochannel cross section geometry is also studied by evaluating the DNA elongation in square, rectangular, and triangular channels. We demonstrate that coupling electrostatically interacting walls with a triangular geometry is an efficient way to stretch DNA molecules at the scale of hundreds of nanometers. The paper reports experimental observations of λ-DNA molecules in poly(dimethylsiloxane) nanochannels filled with solutions of different ionic strength. The results are in good agreement with the theoretical predictions, confirming the crucial role of the electrostatic repulsion of the constraining walls on the molecule stretching.
[http://dx.doi.org/10.1063/1.4904008]

I. INTRODUCTION

The static and dynamic properties of a polyelectrolyte confined in a nanochannel differ from the bulk, and the effects related to confinement are exploited for a variety of biomedical applications. As an example, many separation techniques are based on entropic effects that arise when biopolymers are forced (e.g., by an electric stimulus or a pressure gradient) to interface with nanostructures with different size or topology.[1–6] Moreover, biosensing and single molecule analysis can be achieved by using nanopores[7–11] that allow the detection of biomolecules by means of electrical measurements. Recent works[12–17] have also shown that by elongating DNA molecules in nanochannels, it is possible to optically map DNA strands. *DNA barcoding* is one of the most promising techniques for genome mapping: the DNA is labeled with a fluorescent probe that binds the chain in specific sites. The distance between the positions of labeled DNA is measured by unwinding the molecules in nanochannels.

For all these applications, it is of fundamental importance to know the conformation that a DNA molecule acquires inside nanochannels and in the case of applications such as barcoding,

[a)]Electronic mail: manneschi@ieiit.cnr.it

it is also required that the DNA does not form hairpins or more generally does not coil. This means that at least one size of the confining structures must be below the persistence length P of the molecules. Since, in standard buffer conditions, the persistence length of DNA is around 50 nm,[18] the necessity to strongly extend the molecules faces the difficulty of manufacturing suitable nanostructures. This difficulty is even more severe when one wants to use smart and low cost materials, like elastomers, that can extend the capabilities of the device.[19] Several fabrication techniques have been developed in order to obtain soft and low cost nanostructured devices. Examples include track-etching, which is the most commonly used production technique for polymeric nanopores,[20] REplica Moulding (REM) of nanostructures patterned on a silicon master with a Focused Ion Beam (FIB),[21] formation of nanocracks,[22] and wrinkles[23] on the surface of a stiff polymeric layer, tunnel cracking[24] of a brittle layer sandwiched between elastomeric substrates, and the spontaneous collapse of elastomeric microstructures.[25] Despite the fact that these manufacturing methods allow the realization of sub-micron polymeric structures, reaching scales below 50 nm remains challenging. Recently, several strategies were proposed to overcome the difficulty of linearising polyelectrolytes. An effective method consists of mechanic modulation of an elastomeric nanochannel by compression.[10,22,26] In this context, Huh *et al.*[22] reported dynamical trapping of single DNA molecule in 70 nm deep nanochannels. Another approach, which does not depend on the elastic properties of the material of the confining structures, changes the static and dynamic properties of free and confined molecules by taking advantage of electrostatic intramolecular interactions that become important when DNA is diluted in a low ionic solution.[27–29] Under such conditions the effective persistence length and the effective thickness of the strands increase. As an example, Jo *et al.*[13] achieve larger elongation for genome mapping in 100 nm nanoslits, and Kim *et al.*[30] demonstrate DNA stretching even close to 90% of its contour length also in 250 nm × 400 nm channels.

The dependence of the DNA conformation on the ionic strength of the solution for different conditions of confinement can be also characterized by means of numerical simulations.[30–33] In the most commonly used model, only intra-molecular electrostatic forces are considered, i.e., only the case of a non-polarizable channel[34] is analyzed. However, materials such as poly(dimethylsiloxane) (PDMS) and glass, which are commonly used for creating nanostructured devices, acquire a negative surface charge when immersed in an aqueous solution at physiological pH.[35,36] For this reason, it is of great interest to study how the surface charge on nanochannel walls influences the behaviour of confined DNA chains. The way a repulsively charged channel influences the conformation of flexible and semi-flexible polyelectrolytes was studied by Jeon and Chun[37,38] in the case of a slit-like confinement. They concluded that the wall repulsion has a non-negligible effect on the elongation of chains. We have recently analyzed the influence of the shape of triangular polymeric nanochannels on the elongation of DNA chains at high ionic strength both experimentally and numerically.[39] The simulations revealed that a triangular geometry allows to achieve a large molecular extension due to entropic depletion near the sharp corners of the channel, in agreement with recent results of Reinhart *et al.*[40]

Here, we compare the conformation of the DNA confined in nanochannels with different cross section geometries (square, rectangular, and triangular) and with negatively charged walls. This study is conducted by coupling finite element and Monte Carlo methods. Finite Element Methods (FEM) analysis is used to study the electric potential induced by charged walls, that is hence inserted in Monte Carlo (MC) simulations, in which the DNA molecule is described by a coarse-grained model. Although at high ionic concentrations the elongation of DNA does not significantly depend on the electrostatic interactions between the DNA and the nanochannel, at low concentrations the effect of repulsion from charged walls is important and can be exploited to increase the confining capabilities of the nanostructures. We also report experimental results of λ-DNA elongation in polymeric nanochannels with a triangular cross section. The DNA was labeled with a fluorescent dye and optically detected at various ionic strength of the buffer solution. The experimental results show good agreement with theoretical prediction, thus confirming the crucial role of the electrostatic interactions between DNA and wall.

II. METHODS

A. Simulation details

The conformation of DNA when confined in a polarizable nanochannel was studied by coupling FEM with MC techniques. The electric potential $\phi(x,y)$, generated by charged walls, depends on the ionic strength of the solution that is directly related to the bulk volume density n_i^{∞} of the i-th specie of ions and can be evaluated with a mean field approach by using COMSOL Multiphysics to solve the Poisson-Boltzmann equation

$$\nabla^2\phi = -\frac{e}{\epsilon_0\epsilon_r}\sum_i z_i n_i^{\infty}\exp(-z_i e\phi/k_B T), \tag{1}$$

where e is the electron charge, ϵ_0 is the permittivity of free space, ϵ_r is the relative permittivity ($\epsilon_r = 78.5$ for water), z_i and n_i are the valency and the volume density of the i-th species of ions, respectively, k_B is the Boltzmann constant, and T is the absolute temperature. We used a two dimensional formulation for a monovalent solution of KCl and studied the system for three values of the ionic strength C: 0.1 M, 0.01 M, and 0.001 M. The surface charge density, σ, was set constant for all values of C and equal to that evaluated for poly(dimethylsiloxane) ($\sigma = -5.15 \times 10^{-4}\,\mathrm{C/m^2}$).[38] However, the experimental observations were performed just after the exposure of the polymeric stamp to oxygen plasma. This treatment temporarily modifies the surface properties of PDMS and changes significantly σ. Therefore, for a correct comparison between simulations and optical acquisitions, we measured σ (see Fig. 1 in the supplementary material[41] for details), obtaining $\sigma = -0.5\,\mathrm{C/m^2}$.

In order to validate the model, we compared our numerical data with the analytical prediction reported by Yang *et al.*[42] for a square channel. We obtain a perfect match, as reported in Fig. 2 in the supplementary material.[41]

Figure 1 shows examples of numerical results for a triangular nanochannel (height $h = 50$ nm, base $a = 200$ nm, $\sigma = -5.15 \times 10^{-4}\,\mathrm{C/m^2}$). As expected, $\phi(x,y)$ changes as the ionic strength varies: by lowering the ionic strength of the solution, it decays slowly and extends

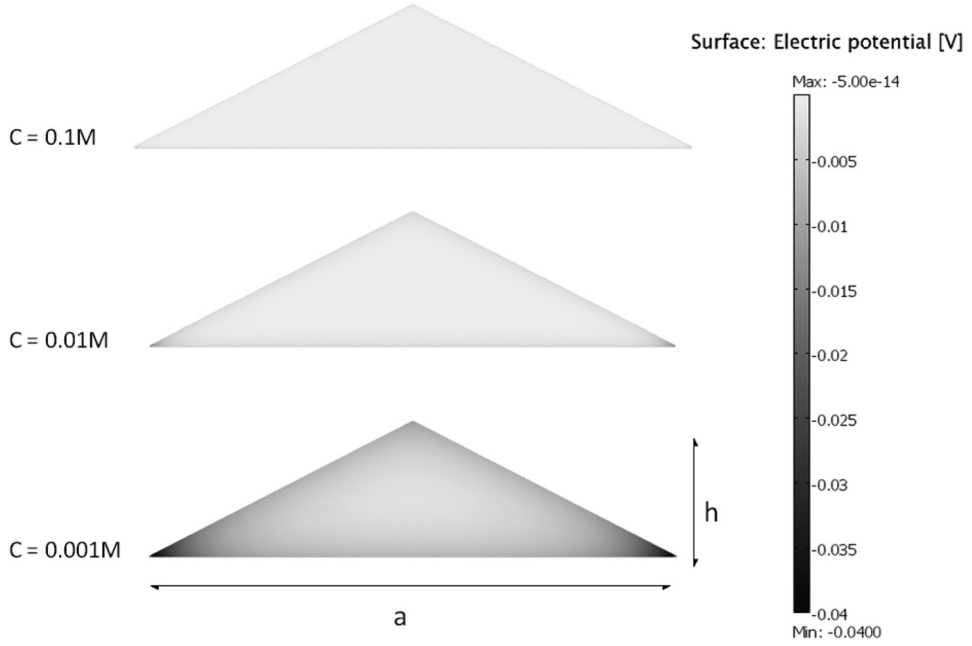

FIG. 1. Electrostatic potential along the cross-section of a triangular charged nanochannel ($h = 50$ nm, $a = 200$ nm, and $\sigma = -5.151 \times 10^{-4}\,\mathrm{C/m^2}$); data obtained with Comsol Multiphysics software. Three different solution concentrations (0.1 M, 0.01 M, and 0.001 M) are shown.

farther away from the walls. The same examples in colour mode are reported in Fig. 3 in the supplementary material.[41]

The Comsol Multphysics software provides a solution of $\phi(x,y)$ evaluated on each node of the mesh. In the Monte Carlo algorithm, the cross section was divided in bi-dimensional cells. A mean value $\phi(cell)$ was attributed to each cell by averaging over all the nodes belonging to it. A table of all the cell sizes, depending on the channel geometry and channel dimensions, is reported in Table I of the supplementary material.[41]

The static behaviour of a confined DNA molecule was modeled via off-lattice simulations and by using Monte Carlo methods. A description of the coarse grained model for the DNA is illustrated in Fig. 4 in the supplementary material.[41] The strand was described by N beads connected by $N-1$ rods of fixed length $l_0 = 5\,\text{nm}$ resulting in a contour length equal to $L_c = l_0(N-1)$. Most of simulations were performed setting $N = 100$, which correspond to 500 nm in length. In order to compare simulation and experimental results, the number of beads was set equal to 4400, which correspond to a length L_c of 22 μm. The total energy U_{tot} of the system depends both on bead-bead and bead-wall interactions. In our model it consists of four terms,

$$U_{tot} = U_{bend} + U_{WCA} + U_{DH} + U_{bw}. \tag{2}$$

The first three terms on the right side of Eq. (2) describe intra-chain interactions, while the last one the electrostatic repulsion between the chain and the wall of the channel.

The term U_{bend}, a bending potential for a Kratky-Porod chain, takes into account the bending rigidity of DNA. It consists in an energy penalty if the angle θ formed by three consecutive beads differs from zero,

$$\frac{U_{bend}(\theta)}{k_BT} = \frac{b}{k_BT}(1-\cos\theta), \tag{3}$$

where b is the bending parameter. The bending parameter and the bare persistence length P_0 are related by[43]

$$P_0 = -l_0/\log\left[\coth\left(\frac{b}{k_BT}\right) - \frac{k_BT}{b}\right]. \tag{4}$$

We set $\frac{b}{k_BT} = 9.73$ to mimic the bare persistent length of 46.1 nm, a value that was empirically estimated by Dobrynin.[44]

The repulsive part of the Lennard Jones potential of the Weeks-Chandler-Andersen (WCA) form[45] was used for non-neighbouring beads to avoid overlap of beads,

$$\frac{U_{WCA}(r)}{k_BT} = \begin{cases} 4\left[\left(\frac{w}{r}\right)^{12} - \left(\frac{w}{r}\right)^{6} + \frac{1}{4}\right], & \text{if } r < 2^{\frac{1}{6}}w; \\ 0 \quad \text{if } r \geq 2^{\frac{1}{6}}w, \end{cases} \tag{5}$$

where w is the adimensional thickness and r is the distance between the center of two non-neighbouring beads. Here, we set $w = l_0$, i.e., we used a tangent sphere model.

The long range intra-beads electrostatic interactions are usually described by the Debye-Huckel potential

$$\frac{U_{DH}(r)}{k_BT} = \frac{1}{k_BT}\frac{q_b^2}{4\pi\epsilon_0\epsilon_r r}\exp(-r/\lambda_D), \tag{6}$$

where q_b is the charge of a bead, and $\lambda_D = \left(\epsilon_0\epsilon_r k_BT/(2e^2 n_{KCl}^{\infty})\right)^{\frac{1}{2}}$ is the Debye length. Due to the high surface charge of the DNA, our system is not within the range of validity of the Debye-Huckel potential. Stigter[46,47] proposed to use the Debye-Huckel potential by replacing the real charge q_b with an effective one. The effective charge is chosen such that the values of

potential generated by a straight cylinder, evaluated through the Debye-Huckel potential and the Poisson-Boltzmann solution, converge asymptotically. The Stigter model for a DNA chain has been extensively validated.[48–51] The effective charge was tabulated, as linear charge density, by Zhang *et al.*[52] Details are reported in Table II in the supplementary material.[41] To speed up calculations, the link-cell algorithm[53] was used during the evaluation of the excluded volume and electrostatic interactions. We assumed that the electrostatic interactions can be neglected if the beads are separated by more than ten times the Debye length λ_D. Thus, we set the dimension of the cell equal to the maximum between w and 10 λ_D. A hard-wall confinement for the chain in the nanochannel was considered by rejecting trial moves with a distance between the center of the beads and the wall less than $w/2$.

Finally, to take into account the electrostatic interactions between DNA and walls, a bead-wall electrostatic term was inserted to the model

$$\frac{U_{bw}(x,y)}{k_BT} = \frac{q_b\phi(x,y)}{k_BT}. \tag{7}$$

Simulations were performed at room temperature (300 K). The charge of each bead was evaluated by considering that each base-pair has a charge of $-2 \times 0.73\,e$, where e is the elementary charge, and a length of 0.34 nm. Since $l_0 = 5$ nm, we set $q_b = -21.47\,e$ as the value for the charge of each bead. We point out that variations on bead charge due to intercalating dyes, commonly used in tracking experiments for staining molecules, have been neglected.

For each simulation, a chain of N beads was generated completely stretched along the channel axis. Thermalization and statistical averages were obtained by reptation trial moves[54] only, since both in our previous work and in Cifra's one[55] no differences were observed by adding crankshaft/bead-displacement moves. We used the Metropolis Monte Carlo algorithm, where a trial move was accepted if $\Omega > \eta$, where $\Omega = \min(\exp[-\Delta U_{tot}/k_BT], 1)$ is the transition probability depending on the difference in energy ΔU between the trial and the initial state, and η is a random number uniformly distributed in the interval [0, 1). For each simulation of a confined molecule, 5×10^7 Monte Carlo Steps (MCS) were performed in order to get a sufficiently large number of independent samples to obtain a reliable estimate of the average physical quantities. For each simulation, we calculated the number of MCS over which the autocorrelation of the DNA elongation along the channel axis is smaller than 5%, and we used this quantity for sampling. The error bars are smaller than the symbol sizes for all the numerical results shown in the figures.

B. Experimental details

DNA detection measurements were performed by using a polymeric device with nanochannels. The fabrication of the device was based on a double replica molding process. Two microchannels and four reservoirs were patterned on a silicon master by standard lithographic techniques, and an array of nanochannels was produced by focused ion beam milling. Then PDMS (Sylgard 184) was used to replicate the pattern into the polymeric material as described by Fanzio *et al.*[56] Finally, the polymeric replica was treated with oxygen plasma and bonded to a glass coverslip in order to seal the device. Nanochannels were characterized by AFM imaging;[39] they have a triangular shape with depth equal to $h = (230 \pm 10)$ nm, width $a = (2.0 \pm 0.2)$ μm, and length $L_{ch} = (200 \pm 1)$ μm. The layout of the device is shown in Fig. 2(a) while in Figs. 2(b) and 2(c) an optical image of the device and a magnification of the region of the nanochannels are shown.

A DNA solution was prepared by diluting λ-DNA (45.8 kbp) in KCl with a concentration of 0.1 μg/ml and pH = 8. We performed experiments for different values of molarity of the solution, i.e., $C = 0.1$ M, 0.01 M, and 0.001 M. DNA molecules were stained with YOYO-1 (Molecular Probes, Invitrogen Corp.) using a dye to base ratio of 1:4. Experimental and numerical conditions were kept as similar as possible to favour the comparison of the results. For this reason, nothing but stained DNA, such as antiphotobleaching agents, was added to KCl solutions.

The polymeric device was filled with the DNA solution and two Pt electrodes were inserted into two opposite reservoirs. A bias of 2 V was applied with a Keithley 6487 source meter in

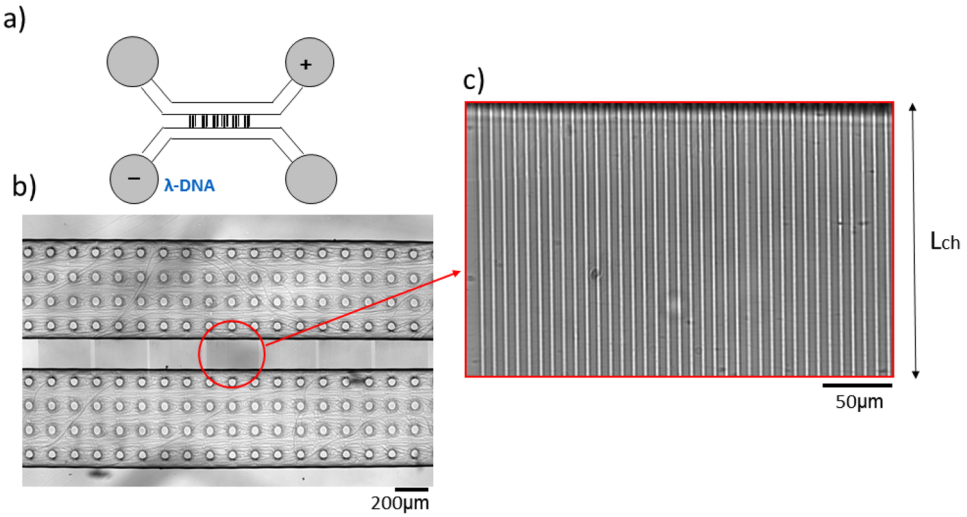

FIG. 2. (a) Layout of the experimental nanofluidic device. Two microchannels are connected by arrays of nanochannels and four reservoirs allow the insertion of the solution. (b) Optical image of a portion of the device and (c) magnification of the region where nanochannels with length $L_{ch} = 200\,\mu$m are patterned.

order to induce the molecules to enter the nanochannels. Acquisitions started two seconds after turning off the electric field, when DNA was relaxed into the channels.[39] The molecule's elongation was observed by using an upright epifluorescence microscope (BX51, Olympus) with a $60\times$ oil-immersion objective (Olympus) and a metal halide lamp (X-cite, Lumen Dynamics, Canada). Images were acquired by using a CCD camera (Fview II, Olympus) with an exposure time of 50 ms.

III. RESULTS AND DISCUSSION

A. Role of the surface charge on the DNA elongation

At low ionic strength, the electrostatic interactions have a significant effect on the conformation of DNA in constrained conditions. In this case in fact, the interactions between the DNA monomers cannot be neglected and intra-bead repulsion results in an increase of the effective persistence length P. In this subsection, we report the role of the channel surface charge on the stretching of confined DNA. We performed numerical simulations of the elongation of a DNA molecule confined in a square nanochannel with neutral and charged walls. In particular, we evaluated the normalized DNA elongation along the channel axis $\langle Z\rangle/L_c$. L_c is the DNA contour length and $\langle Z\rangle$ is the DNA elongation along the channel

$$\langle Z\rangle = \langle \max(z) - \min(z)\rangle, \tag{8}$$

where $\min(z)$ and $\max(z)$ are the component along the channel axis of the center of the leftmost and rightmost beads, respectively. The notation $\langle ...\rangle$ means that all the uncorrelated configurations obtained by MC simulations have been averaged. Figure 3(a) shows $\langle Z\rangle/L_c$ versus the square nanochannel side a for a 500 nm long chain. Three different molar concentrations were considered ($C = 0.1$ M, 0.01 M, 0.001 M). As expected, by lowering the ionic strength of the solution the normalized elongation of the polyelectrolyte increases for both the polarizable and neutral walls. This behaviour is mainly due to the increase of the effective DNA persistence length, which we can estimate by using Dobrynin's empirical equation[44]

$$P = P_0 + P_{el} = \left(46.1 + \frac{1.9195\text{M}}{\sqrt{C}}\right)\text{nm}. \tag{9}$$

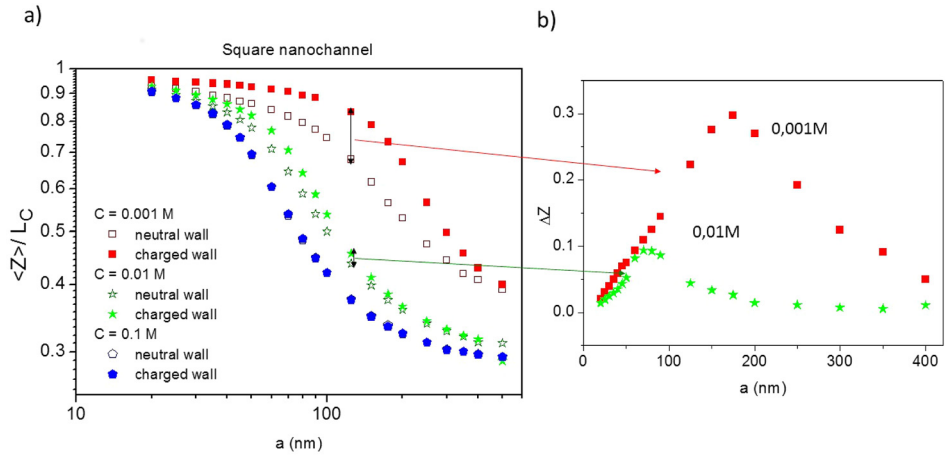

FIG. 3. (a) Comparison between DNA elongation in neutral (empty symbols) and charged (filled symbols) nanochannels with a square cross section: DNA elongation normalized to its contour length ($L_c = 500$ nm) as a function of the nanochannel side a for three salt concentrations (0.1 M, pentagons, 0.01 M, stars, and 0.001 M, squares). (b) Difference between the elongation induced by charged and neutral walls, normalized by the latter as a function of the nanochannel side (salt concentration equal to 0.01 M, stars, and 0.001 M, squares).

The results for 0.1 M, 0.01 M, and 0.001 M are $P_{0.1} = 52.2$ nm, $P_{0.01} = 65.3$ nm, and $P_{0.001} = 106.8$ nm, respectively. We note that at $C = 0.1$ M the electrostatic interactions between the DNA and the channel walls are negligible; in contrast, they become more and more important when lowering the molarity of the solution.

To better visualize this effect, we plot in Fig. 3(b) the difference ΔZ between the elongation induced by a charged and a neutral wall, normalized by the latter, at $C = 0.01$ M and at $C = 0.001$ M. In both cases, ΔZ has a peak when the channel size is slightly larger than the DNA persistence length, i.e., in the region between Odijk's regime[57] and a "transition" regime where back-folding is allowed.[58,59] In fact, at $C = 0.01$ M, ΔZ is maximum at $a = 70$ nm ($\Delta Z_{max} \approx 0.06$), while at $C = 0.001$ M, it is maximum at $a \approx 150$ nm ($\Delta Z_{(max)} \approx 0.1$). In the contrary to the case of neutral channels where the molecules can form hairpins for $a > P$, in the present case the surface charge in the walls induces a reduction of the channel cross section accessible by the molecule, forcing the molecule to stay in a linearized configuration even if a is just slightly larger than P. To check this hypothesis, we compared the DNA elongation count frequencies when setting $C = 0.001$ M and $a = 200$ nm for the neutral and charged channels (Fig. 4). In the neutral case the distribution of the DNA extension is broad indicating that the DNA can explore a wide range of configurations, most of which are characterized by back-folding, as shown in the inset on the left side of Fig. 4. In contrast, in the charged channel the distribution is concentrated at higher values of Z/L_c and is narrower. This indicates that the DNA entropy is lower and the molecules are mainly in extended configurations. Thus, the electrostatic interactions between the molecule and the channel walls can greatly improve the confining capabilities of nanochannel devices, since they produce a larger elongation of the DNA chains and at the same time a reduction in the variance of the molecule's extension.

B. Role of the channel geometry on DNA elongation in neutral and charged-wall nanochannels

Numerical calculations were performed to understand how the channel's cross section shape affects the elongation of a polyelectrolyte in charged-wall nanochannels. Simulations were run for three different geometries: triangular, rectangular, and square. The height (h) of the triangular and rectangular channels was set equal to 50 nm, while the base (a) was varied. The ionic strength of the solution was varied from 0.1 M to 0.001 M while the DNA contour length was set equal to 500 nm. In a previous work,[39] we showed that a good parameter to

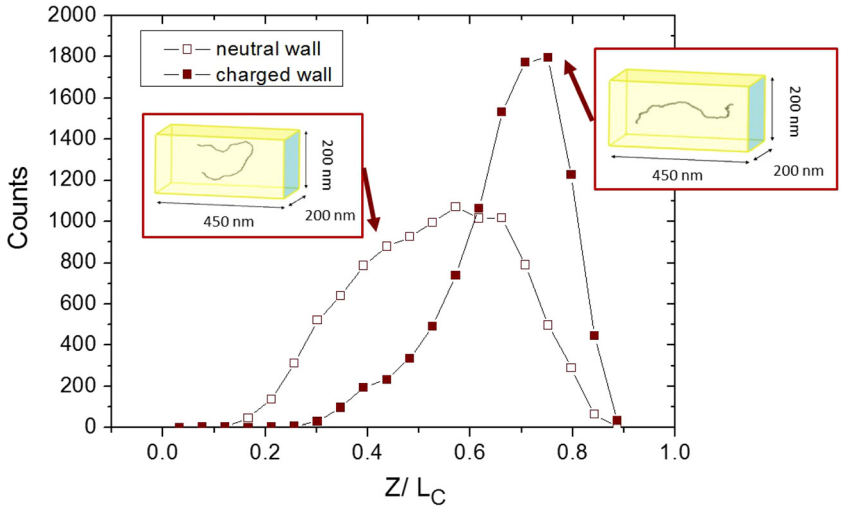

FIG. 4. Comparison between counts related to the normalized DNA elongation ($L_c = 500$ nm) in a square nanochannel (base equal to 200 nm) with charged (filled symbols) and neutral walls (empty symbols) at low ionic strength ($C = 0.001$ M).

describe the geometric effect on the confinement is the effective size of the channel D_{eff} that corresponds to the square root of the area of the channel cross section. For $a/h \approx 1$, $\langle Z \rangle$ does not significantly depend on the channel shape and knowledge of the area of the confining cross section is enough to predict the conformation of the molecule. Differently, for a large aspect ratio a/h of the channel the DNA extension is shape dependent and plotting $\langle Z \rangle$ versus D_{eff} emphasizes the geometric effects.

Results of simulations are shown in Fig. 5, where the normalized DNA elongation is plotted as a function of the effective size D_{eff} of a neutral channel. At high ionic strength ($C = 0.1$ M), considering that the height of the channel, fixed at 50 nm for rectangular and triangular channels, is close to the persistence length of the molecule ($P = 52.2$ nm), we observed a behavior similar to our previous work.[39] In this case, the DNA elongation weakly depends on

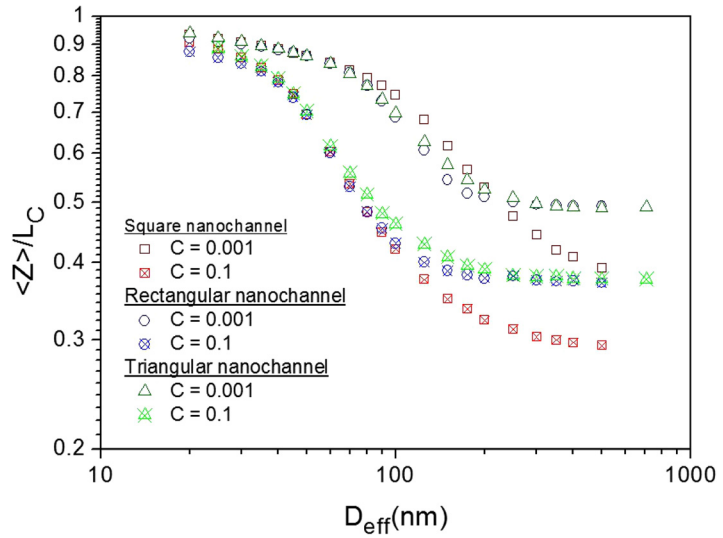

FIG. 5. Normalized DNA elongation ($L_c = 500$ nm) in different nanochannel geometries, i.e., square (squares), rectangular (dots), and triangular (triangles), as a function of D_{eff}, which is the square root of the area of the channel cross section. The nanochannel height for rectangular and triangular channels was fixed equal to 50 nm while the base was varied. The simulations were performed for neutral channels' wall at 0.1 M (crossed symbols) and 0.001 M (empty symbols).

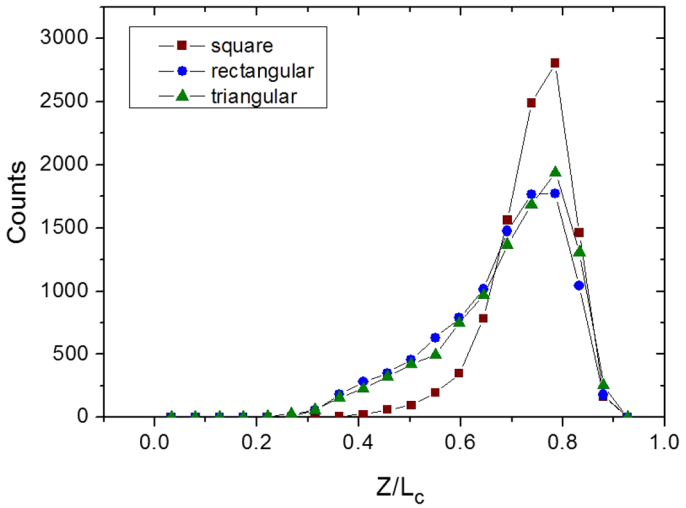

FIG. 6. Frequency count of the normalized extension for the three different geometries. We set $\sigma = 0$ (neutral channels), $D_{eff} = 100$ nm, $h = 50$ nm (for rectangular and triangular channels) and $C = 0.001$ M.

the cross section shape of the channel until the effective size of the constraints is far beyond the persistence length of the molecules. As expected, at weak confinement rectangular and triangular channels stretch the strands more than the square channel.

Decreasing the ionic strength to $C = 0.001$ M, the confining capabilities increase for all geometries due to the increase of the DNA persistence length ($P = 106.8$ nm). In this case, the channel height for the rectangular and triangular channels is lower than the DNA persistence length. For D_{eff} close to P, the square channel induces more confinement than the triangular and rectangular channels. We speculate that this is due to the different aspect ratio of the channels with the same value of D_{eff} but different geometries (as an example, for $D_{eff} = 100$ nm the triangular and rectangular channels have a base equal to 400 nm and 200 nm, respectively). Therefore, while in the square channel the formation of back-folding is suppressed with respect to the fully extended configuration, in rectangular and triangular channels the distribution of the DNA elongation is spread and the molecules can form hairpins along the plane parallel to the base. This assumption is supported by the results reported in Fig. 6, which shows the frequency counts of the extension of a chain confined in the three geometries at $D_{eff} = 100$ nm. All the distributions have a peak for extension at around 80% of the contour length. However, while the distribution in the square channel is narrow and rather symmetric, states with extension at 40% of the contour, which are associated to hairpin configurations, are allowed for both the rectangular and triangular channels. At larger effective size ($D_{eff} > 200$ nm) and $C = 0.001$ M, rectangular and triangular channels induce a slit-like confinement, i.e., the relevant length scale is just the height of the channel (the chain elongation is constant at varying of the width of the channel). In contrast, DNA in square channel tends to its bulk size.

Simulations were also performed by considering nanochannels with charged walls. Figure 7 shows a comparison between the confining capabilities of neutral (same data as in Fig. 5) and charged wall nanochannels: at $C = 0.001$ M, for all the cross section geometries the charged channels confine more with respect to the neutral ones. Moreover, in the case of triangular channels this confinement is particularly strong also for relatively large values of D_{eff}. This behaviour in the case of charged channels can be better observed in Fig. 8, where the DNA elongation frequency count at $D_{eff} = 300$ nm for the three geometries is compared. For rectangular and square channels, the DNA extension is broad indicating that the DNA can explore a large range of configurations, most of which are characterized by back-folding, In contrast, in the charged triangular channel, the distribution is centered at larger values of Z/L_c and it is narrower indicating that the DNA entropy is lower and molecules are mainly in extended configurations. To better explain the stronger confinement capabilities of charged channels, we report

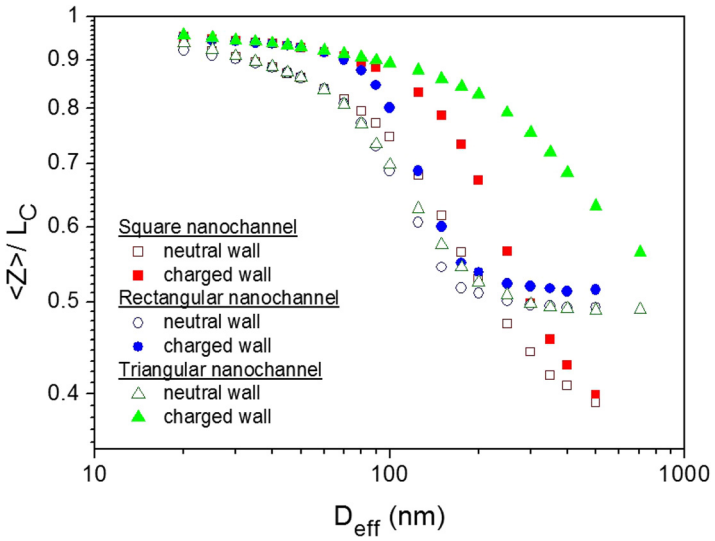

FIG. 7. Dependence of the normalized DNA elongation ($L_c = 500$ nm) on the channel's effective size for square (squares), triangular (triangles), and rectangular (dots) channels at $C = 0.001$ M, for charged (filled symbols) and neutral channels (empty symbols). The channel height for rectangular and triangular channels was set to 50 nm.

in Fig. 9 the bi-dimensional counter plot of the bead position along the channel cross section for the neutral (a)–(c) and charged (d)–(f) channels. It is evident that the depletion zone near nanochannels' walls is larger in the case of charged channels. Moreover, we note that there is a large depletion zone in the sharp corners of the triangular channel that explains the strong confinement capabilities of this geometry.

C. Influence of the contour length on the DNA extension in neutral and charged channels

In the strong confinement regime ($a \ll P$), as predicted by the Odijk's scaling law,[57] the extension of DNA is linear with the molecule contour length. Simulations performed with three different contour lengths, $L_c = 0.25\ \mu$m, $0.5\ \mu$m, and $1\ \mu$m, and two different concentrations, $C = 0.1$ M and $C = 0.001$ M, confirm this linearity both for neutral and charged square channels (see Fig. 10). When the size of the channel approaches to the persistence length, the molecule

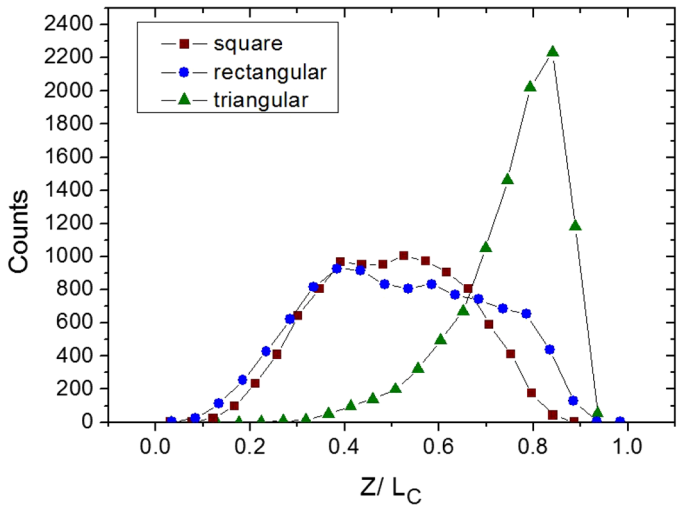

FIG. 8. Comparison between counts of the normalized DNA elongation in square (squares), rectangular (dots), and triangular (triangles) charged nanochannels ($D_{eff} = 300$ nm, $h = 50$ nm for rectangular and triangular channels, $C = 0.001$ M).

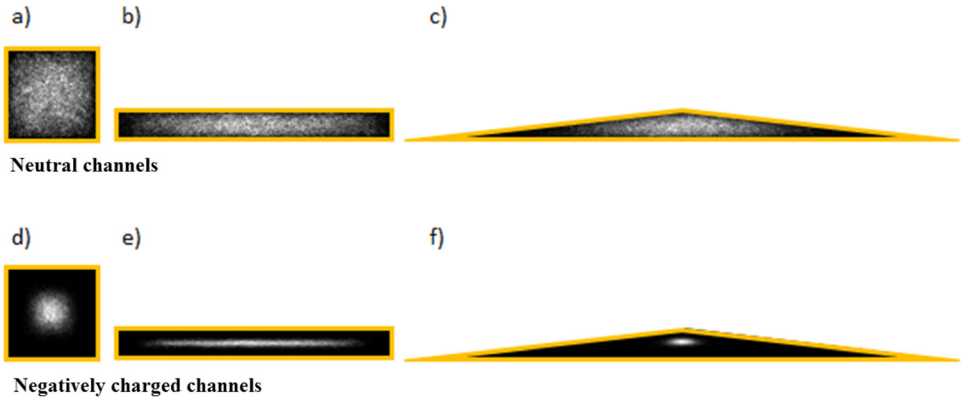

FIG. 9. Distribution of the DNA chain in the cross section of nanochannels with different geometries for both neutral (a)–(c) and charged (d)–(f) walls when the ionic strength of the solution was set to $C = 0.001$ M.

can form back-foldings. For $C = 0.1$ M the extension is still linear with the contour length at $a \approx P$. Only at weak confinement, at which the molecule tends to its bulk conformation, a significant dependence on the contour length is observed. Considering that the molecule stretching is independent on its contour length at high ionic strength, it is possible to compare our results with the experimental observations of λ-DNA molecules reported by Reisner *et al.*[60] in channels with a size up to 80 nm finding a good agreement.

While at $C = 0.1$ M and $a \approx P$ the extension of the molecule is linear with L_c, at $C = 0.001$ M we observe a chain size effect. The chain contour length dependence at low ionic strength is probably related to the low ratio between L_c and P and, as previously observed by Chang and Jo,[34] it is due to the fact that highly contracted DNA conformations are less accessible by the longer DNA molecules. This last observation is also supported by data reported in the supplementary material.[41] Although in the case of low ionic strength the normalized DNA extension slightly varies with L_c, simulations of a 1 μm long molecule inside channels of different shape and size show the same trend displayed in Fig. 7 for a 500 nm long molecule (See the supplementary material[41] for details), i.e., they confirm the importance of surface charge and cross section geometry on the DNA elongation.

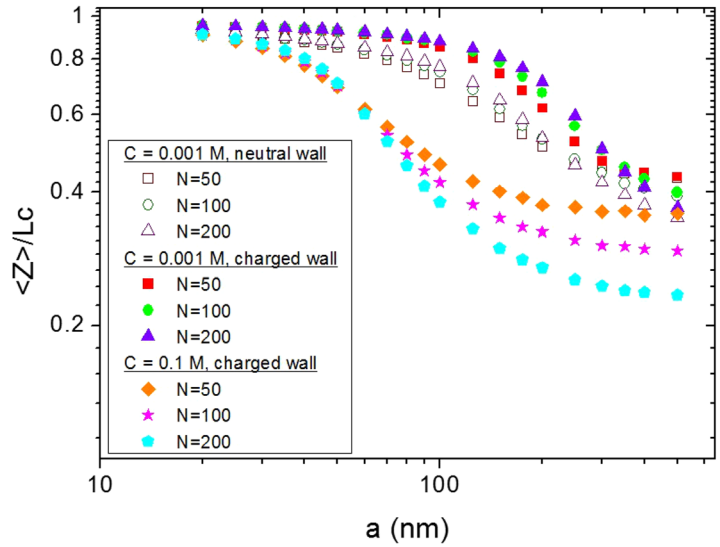

FIG. 10. Dependence of the normalized DNA extension on the molecule contour length L_c in charged (filled symbols) and neutral (empty symbols) square channels at $C = 0.1$ M and $C = 0.001$ M. L_c is 0.25 μm, 0.5 μm, and 1 μm.

D. Experiments and simulations of λ-DNA elongation varying the ionic strength

DNA elongation was experimentally evaluated by visualizing the YOYO-labeled λ-DNA molecules confined inside PDMS nanochannels. The device, as described in the "Experimental Details" subsection, contains triangular nanochannels that have a negative surface charge when filled with KCl solution and pH = 8. Optical images were analyzed with a homemade software that allowed to obtain the extension of the molecules. As expected, Fig. 11 (dots) shows that λ–DNA elongation increases when decreasing the ionic strength of the solution. As an example, optical images of the DNA chains at different salt concentrations can be seen in the inset of Fig. 11. Experimental data were compared with numerical data obtained by considering a triangular nanochannel (base $b = (2.0 \pm 0.2)$ μm, height $h = (230 \pm 10)$ nm) and setting the surface charge $\sigma = -0.5\,\mathrm{C/m^2}$ (stars) and $\sigma = 0$ (triangles). In order to compare numerical and experimental data, the number of beads used for the simulations was increased to N = 4400, corresponding to $L_c = 22\,\mu$m, i.e., the contour length of a stained λ-DNA molecule.

Experimental results agree very well with simulations for $C = 0.1$ M and $C = 0.01$ M, both for neutral and charged channel. For $C = 0.001$, measurements confirm the importance of the electrostatic repulsion from the walls. In fact, the observed stretching of the molecule is much larger than predicted by simulations setting $\sigma = 0$, while fits quite well with numerical calculations for $\sigma = -0.5\,\mathrm{C/m^2}$. We note that simulations for charged channel predict a slightly larger value of the DNA elongation than the one experimentally observed: this difference can be explained by considering that there are sources of errors in the evaluation of the parameters of the electrostatic terms used in the model. These are mainly related to the fact that we have neglected the influence of the staining molecules (YOYO-1) that decreases the DNA charge and to difficulties in the evaluation of the PDMS surface charge because of the well-known recovery of PDMS surface properties after the oxygen plasma treatment. Furthermore, nanochannels are made of both PDMS and glass at the interface with the solution while we used a single value of surface charge that was extrapolated by preliminary measurements of ionic conductance inside a channel. Anyway, although the parameters used in the simulations slightly overestimate the DNA extension, optical data confirm the reliability of the numerical model and the key role of the chain-wall electrostatic interactions in understanding the DNA behaviour in confining channels.

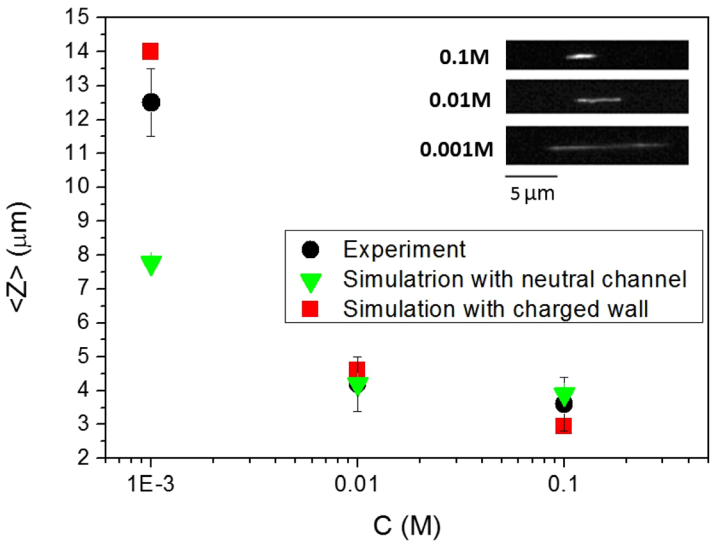

FIG. 11. Mean DNA elongation as a function of the ionic strength C: comparison between experimental results (dots) and simulations in triangular nanochannels with charged (squares) and neutral walls (triangles). The inset shows fluorescence images of the confined YOYO-labeled DNA at different salt concentrations.

IV. CONCLUSION

In this work, finite element calculations and Monte Carlo simulations were coupled in order to study the behaviour of DNA molecules confined in nanochannels with charged walls. The electrostatic interaction is crucial in increasing the DNA elongation by lowering the ionic strength of the solution also in neutral nanochannels. This behaviour is emphasized in the presence of a surface charge even in wide nanochannels: as an example, in a negatively charged 300 nm square nanochannel it is possible to achieve a 50% DNA elongation by inserting a 0.001 M ionic solution. Almost completely stretched molecules are obtained even in 200 nm channels, and the distribution of the DNA extension is narrow indicating that the DNA entropy is low and molecules are mainly in an extended configurations. This effect is amplified in triangular shaped nanochannels due to the depletion zone near nanochannels walls and, in particular, in the sharper corners. The possibility to increase the DNA elongation even in relatively large nanochannels by simply changing the surface charge and the strength of the solution should be useful for applications such as DNA mapping and barcoding, which require large elongation of biomolecules during the analysis. In conclusion, we have also reported experimental results on λ-DNA elongation in polymeric triangular nanochannels with negatively charged walls. Experimental data are in agreement with our numerical data and consolidate the key role of the electrostatic repulsion of the channel in achieving large stretching of the molecules even in fluidic structures just below the micrometer size.

ACKNOWLEDGMENTS

The work has been performed under the HPC-EUROPA2 project (Project No. 1009) with the support of the European Commission-Capacities Area-Research Infrastructures. It has been supported by Ministero dell' Università e della Ricerca (MIUR), Italy, with the National Projects NANOMAX and the FIRB Project NEWTON, and in part by the Academy of Finland through its COMP CoE (No. 251748) and NanoFluid grant, and by the Italian MIUR Flagship Project "InterOmics". We thank Dr. Sahin Buyukdagli for useful discussions.

[1]J. Han and H. G. Craighead, Science **288**, 1026 (2000).
[2]M. Cabodi, S. W. P. Turner, and H. G. Craighead, Anal. Chem. **74**, 5169 (2002).
[3]J. Fu, R. B. Schoch, A. L. Stevens, S. R. Tannenbaum, and J. Han, Nat. Nanotechnol. **2**, 121 (2007).
[4]J. T. D. Bonis-O'Donnell, W. Reisner, and D. Stein, New J. Phys. **11**, 075032 (2009).
[5]S. T. T. Ollila, C. Denniston, M. Karttunen, and T. Ala-Nissila, Phys. Rev. Lett. **112**, 118301 (2014).
[6]T. Ikonen, J. Chem. Phys. **140**, 234906 (2014).
[7]J. J. Kasianowicz, E. Brandin, D. Branton, and D. W. Deamer, Proc. Natl. Acad. Sci. U.S.A. **93**, 13770 (1996).
[8]S. Howorka, S. Cheley, and H. Bayley, Nat. Biotechnol. **19**, 636 (2001).
[9]J. Clarke, H.-C. Wu, L. Jayasinghe, A. Patel, S. Reid, and H. Bayley, Nat. Nanotechnol. **4**, 265 (2009).
[10]P. Fanzio, C. Manneschi, E. Angeli, V. Mussi, G. Firpo, L. Ceseracciu, L. Repetto, and U. Valbusa, Sci. Rep. **2**, 791 (2012).
[11]V. Mussi, P. Fanzio, L. Repetto, G. Firpo, S. Stigliani, G. P. Tonini, and U. Valbusa, Biosens. Bioelectron. **29**, 125 (2011).
[12]R. Riehn, M. Lu, Y.-M. Wang, S. F. Lim, E. C. Cox, and R. H. Austin, Proc. Natl. Acad. Sci. U.S.A. **102**, 10012 (2005).
[13]K. Jo, D. M. Dhingra, T. Odijk, J. J. d. Pablo, M. D. Graham, R. Runnheim, D. Forrest, and D. C. Schwartz, Proc. Natl. Acad. Sci. U.S.A. **104**, 2673 (2007).
[14]W. Reisner, N. B. Larsen, A. Silahtaroglu, A. Kristensen, N. Tommerup, J. O. Tegenfeldt, and H. Flyvbjerg, Proc. Natl. Acad. Sci. U.S.A. **107**, 13294 (2010).
[15]S. F. Lim, A. Karpusenko, J. J. Sakon, J. A. Hook, T. A. Lamar, and R. Riehn, Biomicrofluidics **5**, 034106 (2011).
[16]R. L. Welch, R. Sladek, K. Dewar, and W. W. Reisner, Lab Chip **12**, 3314 (2012).
[17]Y. Wang, W. F. Reinhart, D. R. Tree, and K. D. Dorfman, Biomicrofluidics **6**, 014101 (2012).
[18]P. J. Hagerman, Annu. Rev. Biophys. Biophys. Chem. **17**, 265 (1988).
[19]R. Chantiwas, S. Park, S. A. Soper, B. C. Kim, S. Takayama, V. Sunkara, H. Hwang, and Y.-K. Cho, Chem. Soc. Rev. **40**, 3677 (2011).
[20]A. Mara, Z. Siwy, C. Trautmann, J. Wan, and F. Kamme, Nano Lett. **4**, 497 (2004).
[21]E. Angeli, C. Manneschi, L. Repetto, G. Firpo, and U. Valbusa, Lab Chip **11**, 2625 (2011).
[22]D. Huh, K. L. Mills, X. Zhu, M. A. Burns, M. D. Thouless, and S. Takayama, Nat. Mater. **6**, 424 (2007).
[23]S. Chung, J. H. Lee, M.-W. Moon, J. Han, and R. D. Kamm, Adv. Mater. **20**, 3011 (2008).
[24]K. L. Mills, D. Huh, S. Takayama, and M. D. Thouless, Lab Chip **10**, 1627 (2010).
[25]S.-M. Park, Y. S. Huh, H. G. Craighead, and D. Erickson, Proc. Natl. Acad. Sci. U.S.A. **106**, 15549 (2009).
[26]C. Manneschi, P. Fanzio, E. Angeli, G. Firpo, L. Ceseracciu, V. Mussi, L. Repetto, and U. Valbusa, Microfluid. Nanofluid. **14**, 21 (2013).

[27]W. Reisner, J. P. Beech, N. B. Larsen, H. Flyvbjerg, A. Kristensen, and J. O. Tegenfeldt, Phys. Rev. Lett. **99**, 058302 (2007).
[28]C. Zhang, F. Zhang, J. A. v. Kan, and J. R. C. v. d. Maarel, J. Chem. Phys. **128**, 225109 (2008).
[29]C.-C. Hsieh, A. Balducci, and P. S. Doyle, Nano Lett. **8**, 1683 (2008).
[30]Y. Kim, K. S. Kim, K. L. Kounovsky, R. Chang, G. Y. Jung, J. J. dePablo, K. Jo, and D. C. Schwartz, Lab Chip **11**, 1721 (2011).
[31]Y.-L. Chen, Biomicrofluidics **7**, 54119 (2013).
[32]P.-k. Lin, C.-C. Hsieh, Y.-L. Chen, and C.-F. Chou, Macromolecules **45**, 2920 (2012).
[33]J. Lee, S. Kim, H. Jeong, G. Y. Jung, R. Chang, Y.-L. Chen, and K. Jo, ACS Macro Lett. **3**, 926 (2014).
[34]R. Chang and K. Jo, J. Chem. Phys. **136**, 095101 (2012).
[35]I. Wong and C.-M. Ho, Microfluid. Nanofluid. **7**, 291 (2009).
[36]S. H. Behrens and D. G. Grier, J. Chem. Phys. **115**, 6716 (2001).
[37]J. Jeon and M.-S. Chun, J. Chem. Phys. **126**, 154904 (2007).
[38]J. Jeon and M.-S. Chun, Korea-Aust. Rheol. J. **19**, 51 (2007).
[39]C. Manneschi, E. Angeli, T. Ala-Nissila, L. Repetto, G. Firpo, and U. Valbusa, Macromolecules **46**, 4198 (2013).
[40]W. F. Reinhart, D. R. Tree, and K. D. Dorfman, Biomicrofluidics **7**, 024102 (2013).
[41]See supplementary material at http://dx.doi.org/10.1063/1.4904008 for additional information on the experimental characterization and on the convalidation, settings, and results of simulations.
[42]Marcos, C. Yang, T. N. Wong, and K. T. Ooi, Int. J. Eng. Sci. **42**, 1459 (2004).
[43]C. Micheletti, D. Marenduzzo, and E. Orlandini, Phys. Rep. **504**, 1 (2011).
[44]A. V. Dobrynin, Macromolecules **39**, 9519 (2006).
[45]J. D. Weeks, D. Chandler, and H. C. Andersen, J. Chem. Phys. **54**, 5237 (1971).
[46]D. Stigter, J. Colloid Interface Sci. **53**, 296 (1975).
[47]D. Stigter, Biopolymers **16**, 1435 (1977).
[48]A. A. Brian, H. L. Frisch, and L. S. Lerman, Biopolymers **20**, 1305 (1981).
[49]E. G. Yarmola, M. I. Zarudnaya, and Y. S. Lazurkin, J. Biomol. Struct. Dyn. **2**, 981 (1985).
[50]S. Y. Shaw and J. C. Wang, Science **260**, 533 (1993).
[51]V. V. Rybenkov, N. R. Cozzarelli, and A. V. Vologodskii, Proc. Natl. Acad. Sci. U.S.A. **90**, 5307 (1993).
[52]Y. Zhang, H. Zhou, and Z.-C. Ou-Yang, Biophys. J. **81**, 1133 (2001).
[53]I. Gerroff, A. Milchev, K. Binder, and W. Paul, J. Chem. Phys. **98**, 6526 (1993).
[54]F. T. Wall and F. Mandel, J. Chem. Phys. **63**, 4592 (1975).
[55]P. Cifra and T. Bleha, Soft Matter **8**, 9022 (2012).
[56]P. Fanzio, V. Mussi, C. Manneschi, E. Angeli, G. Firpo, L. Repetto, and U. Valbusa, Lab Chip **11**, 2961 (2011).
[57]T. Odijk, Macromolecules **16**, 1340 (1983).
[58]P. Cifra, Z. Benkova, and T. Bleha, J. Phys. Chem. B **113**, 1843 (2009).
[59]W. Reisner, J. N. Pedersen, and R. H. Austin, Rep. Prog. Phys. **75**, 106601 (2012).
[60]W. Reisner, K. J. Morton, R. Riehn, Y. M. Wang, Z. Yu, M. Rosen, J. C. Sturm, S. Y. Chou, E. Frey, and R. H. Austin, Phys. Rev. Lett. **94**, 196101 (2005).